**International Journal of Electrical and Computer Engineering (IJECE)**
Vol. 15, No. 5, October 2025, pp. 4692~4704
ISSN: 2088-8708, DOI: 10.11591/ijece.v15i5.pp4692-4704 

# Bone-Net: a parallel deep convolutional neural network-based bone fracture recognition

**Md. Hasan Imam Bijoy[1,2], Nusrat Islam Kohinoor[3], Syeda Zarin Tasnim[3], Md. Saidur Rahman Kohinoor[3,4]**
[1]Health Informatics Research Lab (HIRL), Daffodil International University, Dhaka, Bangladesh
[2]Department of Computer Science and Engineering, Daffodil International University, Dhaka, Bangladesh
[3]Department of Computer Science and Engineering, Leading University, Sylhet, Bangladesh
[4]Department of Information and Computer Science, King Fahd University of Petroleum and Minerals, Dhahran, Saudi Arabia

**Article Info**

***Article history:***

Received Mar 23, 2024
Revised May 25, 2025
Accepted Jun 30, 2025

***Keywords:***

Bone fracture
Canny edge detection
Convolutional neural network
MobileNet-V2
Parallel deep convolutional neural network

**ABSTRACT**

Many people suffer from bone fractures, which can result from minor accidents, forceful blows, or even diseases like osteoporosis or bone cancer. In the medical realm, accurately identifying bone fractures from X-ray images is paramount for effective diagnosis and treatment. To address this, a comparative study is conducted utilizing three distinct models: a traditional convolutional neural network (CNN), MobileNet-V2, and a newly developed parallel deep convolutional neural network (PDCNN). The primary aim is to evaluate and contrast these models in terms of precision, sensitivity, and specificity for diagnosing bone fractures. X-ray images of fractured and non-fractured bones are sourced from Kaggle and subjected to various image processing techniques to rectify anomalies. Techniques such as cropping, resizing, contrast enhancement, filtering, and augmentation are applied, culminating in canny edge detection. These processed images are then used to train and test models. The results showcased the superior performance of the newly developed PDCNN model, achieving an impressive accuracy of 92.89%, surpassing both the traditional CNN and pretrained MobileNet-V2 models. A series of ablation studies are conducted to fine-tune the hyperparameters of the PDCNN model, further validating its efficacy. Throughout the investigation, PDCNN consistently outperformed MobileNet-V2 and traditional CNN, underscoring its potential as an advanced tool for streamlining bone fracture identification.



***Corresponding Author:***

Md. Hasan Imam Bijoy
Department of Computer Science and Engineering, Daffodil International University
Daffodil Smart City, Dhaka-1216, Bangladesh
Email: hasan15-11743@diu.edu.bd

## 1. INTRODUCTION

A mineral made of calcium is called bone [1]. Human bone provides a mechanical structure for the human body [2]. It maintains calcium homeostasis and substantial storage of phosphate, magnesium, potassium, and bicarbonate. Human bone also helps in muscle activities [3]. One of the most interesting natural composite materials is human cortical bone, which acts as a structural foundation that can withstand injury and allows the human body to self-repair. The mechanical characteristics of bone enable it to withstand fracture under diverse physiological loading conditions [4]. A few of these conditions that lead to bone diseases are vitamin-D insufficiency, osteoporosis, Paget's disease of the bones, and many more. The amount and quality of bone tissue in the human skeleton start to decline after reaching peak bone mass in the

third or fourth decade of life [5]. Among the most common injuries in today's world are bone fractures. About 8.9 million people experience this disorder each year [6], and the consequences of leaving a fracture untreated may end in death or permanent damage by several types of bone fracture as shown in Figure 1. The doctors bear a great deal of responsibility for this, as they assess lots of X-ray images daily basis. The majority of the technology used for the initial diagnosis is X-rays, a modality that has been around for more than a century and is still widely used. Medical professionals find it difficult to assess X-ray images for many reasons, like the fact that X-rays may obscure certain unique characteristics of the bone or that it takes extensive training to accurately identify the various kinds of fractures. A precise classification of the fracture among standard types is crucial for both the future outlook and the effectiveness of the treatment [7].

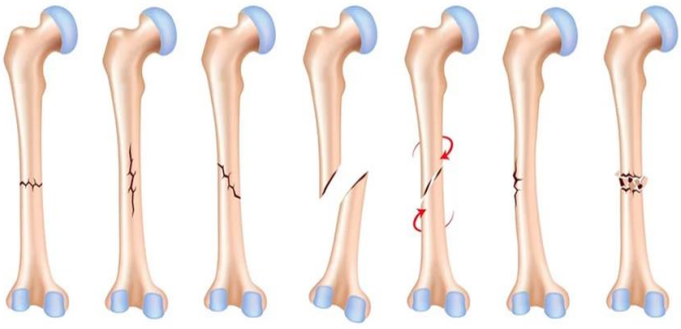

Figure 1. Several types of fracture in bone

Many advances in technology are making it easier to diagnose bone fractures in today's world. Automated image processing models, such as artificial intelligence (AI), deep learning (DL), and machine learning (ML), are quick and reliable for identification, localization, and classification [8]. Determining the precise location of a fracture and its degree of impact might be beneficial. The discipline of computer-aided diagnosis is an emerging field of research where computer technologies are used to offer prompt and precise diagnosis. It uses X-ray images and preprocesses them as needed to detect fractures in the bones [9]. They are getting better with each passing day as a result of learning from labeled data [10].

Several works have been discussed, including the following, Luis and Ruano [11] suggested a computer-aided system for bone fracture detection. Although X-ray pictures are typically used to diagnose bone fractures, and suggested an approach that uses computers to help detect bone fractures. Achieved 89% classification accuracy by utilizing a variety of techniques for fracture recognition, bone line detection, and speckle reduction. It is limited to stress fractures, and this computer-aided approach is unable to classify complex fractures accurately.In 2015, Anu *et al.* [12] presented work using preprocessing techniques to reduce noise from the photos and transform the RGB X-ray images to grayscale using a median filter. They then detected the edge of the image by using the Sobel edge detector. They used the gray level co-occurrence Matrix (GLCM) to extract the feature. Finally, the data were divided into fractured and non-fractured categories using a variety of classifier types, including decision trees (DT), neural networks (NN), and meta-classifiers. There are 40 photos in the collection, 20 of which have fractures and 20 of which do not. They achieved the best accuracy in the meta-classification algorithm, at 85 percent. Tripathi *et al.* [13] stated that the location of small or hairline femur fractures is the main topic of this paper. To determine whether or not there is a fracture, they employed SVM. 30 X-ray images compose the dataset. The logarithmic operator is employed to enhance photos, and median and average filtering are used to eliminate noise from images. Morphological operations and the sobel edge detection approach are employed for feature extraction. They obtained 84.7 percent accuracy in classifying the data using support vector machines (SVM) into fractured and non-fractured categories. Sinthura *et al.* [14] suggested a convolutional neural network (CNN) to detect bone fractures. They took an x-ray image as input, then preprocessed it using a median filter, and the preprocessed image was applied to the discrete wavelet transforms (DWT) stage, which is used to find the edge in each channel. Then the output is compared with the database with neural networks, which gives the output.

Vasilakakis *et al.* [15] suggested fuzzy phrases (FP) for detection. This work aims to use the wavelet fuzzy phrases (WFP) approach to identify bone fractures using x-ray pictures. The accuracy of the classifying approach was 84%. Yadav and Sandeep [16] built a deep CNN model to actively classify fractured or healthy bones. After augmentation, the dataset had a size of 4000, where 2000 is a healthy bone and 2000 is cancerous, they used five-fold cross-validation and have the best accuracy of all, scoring 92.44 percent.

Rao *et al.* [17] proposed a method to detect bone fractures. Their dataset had 300 X-ray pictures, and they achieved 90% accuracy by using a back propagation neural network (BPNN) and SIFT feature extraction. In 2020, Karimunnisa *et al.* [18] suggested a model using 900 X-ray pictures, of which 400 were normal and 500 were fractured. Initially, input X-ray pictures are transformed into grayscale images. Their BPNN provides an improved classification rate of 91 percent. Pathare *et al.* [19] employ many processing approaches, including segmentation, edge detection, and feature extraction. Bekkanti *et al.* [20] suggested the Harris corner detection technique, which is a traditional computer vision technique related to feature detection and traditional image processing to detect bone fractures. There were two hundred non-fractured and three hundred fractured X-ray images in their collection. The input x-ray images are preprocessed using m3 filtering. segmented using canny edge detection, features extracted using Harris corner detection, and lastly categorized as fractured or not. They contrasted their efforts using SURF with BPNN and MLP-based BPNN. While SURF using BPNN yields an accuracy of 85 percent, MLP-based BPNN yields an accuracy of 85 percent, and their suggested approach yields a 94 percent accuracy. In 2022, Samothai *et al.* [21] presented advanced CNN YOLO models in this work, where the widely used YOLO-X and YOLO-R models were implemented. With 76 percent confidentiality, YOLO-X can locate fractures with great accuracy. However, YOLO-R exhibits inaccurate fracture location detection. Kosrat and Hawezi [22] analyze various ML classifiers and assist surgeons in accurately diagnosing bone fractures. They employed a filtering technique to remove noise and preprocessing to convert the RGB images to grayscale. In this study, SVM is found to be the best.

Certain issues persist in the current state of bone fracture detection, necessitating improvements in accuracy to enhance detection efficacy, as outlined in Table 1 and the aforementioned study. The augmentation of the dataset is imperative, requiring the inclusion of high-quality photos. This study utilizes a dataset comprising a substantial number of bone fracture images, implementing canny edge detection during preprocessing to optimize results. Despite the growing accessibility of machine-aided bone fracture detection, accuracy remains a concern, often leading to false positives. The identification of fractures in the absence of actual occurrences is a prevalent problem, attributed to the limited volume of data and inaccuracies in the labeling of training data. Addressing these challenges, this research focuses on refining training and testing data by introducing a newly customized parallel deep learning model with parameter customization. Notably, publicly available datasets frequently lack flawless preprocessing and accurate labeling, necessitating the incorporation of additional labeled data to augment inputs for the model. To ensure an adequate supply of high-quality data, edge detection algorithms are employed during data preprocessing. The contributions of this study can be summarized as follows:

a. Correcting anomalies in the dataset through several image processing technique involves employing a range of image processing techniques, such as cropping, resizing, contrast enhancement, filtering, augmentation, and culminating in canny edge detection.
b. The study introduces a novel and tailors parallel deep convolutional neural network (PDCNN) model, designed to surpass the existing literature by enhancing accuracy in bone fracture detection.
c. A comparative evaluation is conducted among three CNN-based models—CNN, MobileNet-V2, and the newly proposed PDCNN. Four cases of ablation studies is carried out to validate the proposed PDCNN model. The objective is to identify the most effective model for bone fracture recognition through a thorough analysis of their performance.

Table 1. Summarized literature review of bone fracture recognition using machine learning models

| Study | Data | Preprocessing Technique | Model | Accuracy | Limitations/Remarks |
|---|---|---|---|---|---|
| [11] | 44 | Canny edge detection | SNAKE | 89% | Only detects stress fractures and is unable to classify complex fractures accurately. There are not many images in the dataset. |
| [12] | 40 | Sobel edge detector | Meta Classifier | 85% | The dataset was not good. |
| [13] | 30 | Sobel edge detector | SVM | 87.5% | The dataset was not good. |
| [14] | NM | discrete wavelet transforms (DWT) | CNN | 79% | The dataset was not given. |
| [15] | 300 | NM | WFP | 84% | This was the early stage of fuzzy phrases; additional development is required before they can be reliably detected. |
| [17] | 300 | M3 filter | SIFT + BPNN | 90% | HTBFD, ANN, and other algorithms are useful tools for improving fracture placement. |
| [18] | 900 | Canny Edge Detection and Conservative Filtering | BPNN | 91% | The dataset contains many types of bone shapes, which may become confusing. |
| [19] | 20 | NM | HTM | 75% | An X-ray of the skull, pelvis, and spinal column was not able to be obtained. |
| [22] | 270 | Canny edge detection | SVM | NM | It only compared the models. |

a. NM: Not mentioned

## 2. RESEARCH METHOD

This study centers on the detection of bone fractures in X-ray images through the utilization of a CNN-based model. The development of the proposed system involves sequential steps, including data collection, image pre-processing, and fracture recognition using CNN models. The schematic representation of the working process is outlined in Figure 2.

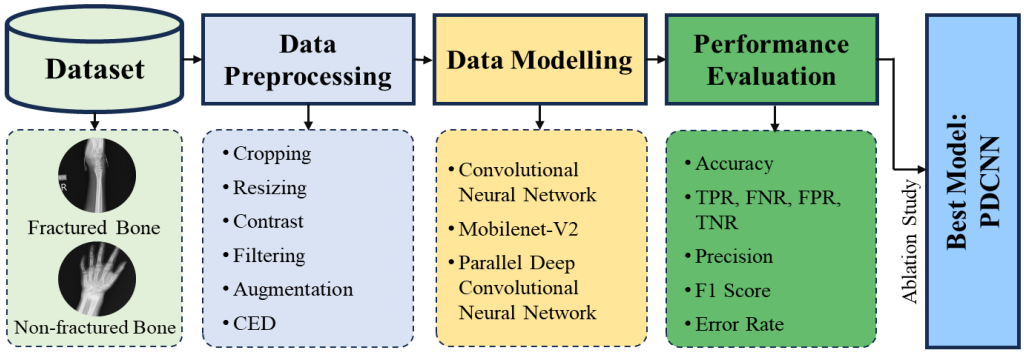


Figure 2. The workflow diagram of proposed study

### 2.1. Dataset description

This study makes use of a public dataset of bone fracture and non-fractured x-ray images. To keep things simple, the publicly available dataset of binary-class bone fracture and non-fracture x-ray images was obtained using the Kaggle platform; for the sake of this paper, this data is referred to as the "bone fracture dataset" [23]. It is employed in the creation of an image classifier that identifies bone fractures in given x-ray pictures. There are 1899 photos identified in the testing class (fracture and non-fracture) and 8,884 images in the training class (fracture and non-fracture). The images were not the same size, and some of them included anomalous data in addition to being unclear. The sample image of fractured bone and fresh bone of x-ray image is given in Figure 3. Figure 3(a) represents the fractured bone, while Figure 3(b) depicts the non-fractured bone.


(a) (b)

Figure 3. The sample image of (a) fractured bone, and (b) non-fractured bone

### 2.2. Data preprocessing

In the realm of bone fracture identification, a crucial step in the research applications of computer vision and image processing involves image preprocessing. This process serves to enhance the quality of images, reduce noise levels, rectify distortion, and prepare the images for subsequent analysis [16]. The following are key strategies (see outcome of Figure 4(a) to 4(h)) employed in this study, along with explanations.

#### 2.1.1. Cropping

In bone fracture identification, cropping is a prevalent image processing technique utilized to extract the region of interest (ROI) within an image [24]. This facilitates the isolation of relevant anatomical structures for more accurate analysis, disregarding unnecessary elements. The output of cropping from the raw picture of Figure 4(a), can be seen in Figure 4(b).

#### 2.1.2. Resizing

Resizing plays a vital role in standardizing the dimensions of images within a dataset. This ensures uniformity, facilitating efficient processing and analysis [25]. It also aids in accommodating variations in image resolutions commonly encountered in medical imaging. Resizing is employed to standardize the dimensions of images, ensuring uniformity across the dataset with 227×227 pixels and the output shown in Figure 4(c).

#### 2.1.3. Enhancing contrast

Enhancing contrast is crucial to accentuate subtle details within the images [26]. This allows for better differentiation between healthy and fractured bone structures, enhancing the overall interpretability of the images. After enhancing the image quality, Figure 4(d) displays the image with improved visual clarity.

#### 2.1.4. Filtering

Filtering is employed to emphasize relevant structural details while suppressing noise. By selectively enhancing certain image characteristics, filtering contributes to the improvement of image clarity and the extraction of essential information [18]. After filtering and enhancing the essential features, the image is displayed in Figure 4(e).

#### 2.1.5. Canny edge detection

Canny edge detection (CED) is an advanced image processing technique used in computer vision to identify edges and boundaries within an image [27]. It was developed to address the challenges of edge detection by providing accurate and reliable results while minimizing false positives. In the context of bone fracture recognition using computer vision and image processing, canny edge detection plays a crucial role in highlighting prominent contours and edges within medical images. This technique enhances the visualization of structural details in bone images, making it particularly valuable for pinpointing fractures and irregularities in the bone structure which is displayed in Figure 4(f).

#### 2.1.6. Augmentation

Augmentation is crucial for enhancing the robustness of bone fracture identification models. By exposing the model to diverse orientations, scales, and perspectives, it becomes more adept at accurately identifying fractures under a range of conditions, contributing to improved generalization and performance [28]. In this study, some primary image augmentation method is used such as rotation, flipping, zooming, and shearing and the outcomes of the filtered images and CED are displayed in Figure 4(g) and Figure 4(h), respectively.

After undergoing extensive image processing, the raw image is subjected to contrast enhancement, as illustrated in Figure 4(a) to 4(h). The dataset comprises more than 10, 783 images categorized into fractured and non-fractured classes, exhibiting a near balance between the two. Following an 85:15 split for training and testing, the dataset consists of 8884 images in the training set and 1899 images in the test set.

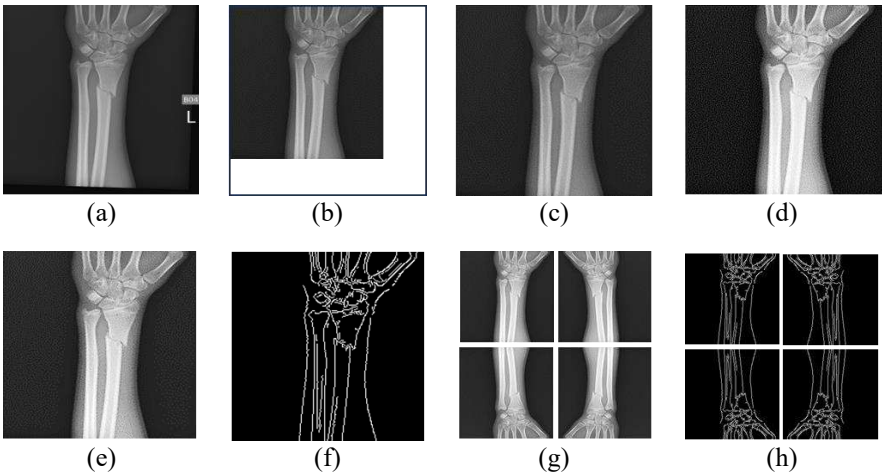


Figure 4. Several image processing applied into (a) raw image and getting (b) cropping image, (c) resize image, (d) enhance contrast, (e) filtering, (f) augmentation on filtered image, and (g) canny edge detection and (h) augmented CED image to increase the size of the dataset

### 2.3. Model implementation

Following the preprocessing phase, this study endeavors to construct a bone fracture recognition system by employing CNN based models. In pursuit of high accuracy, we explore a variety of models including the traditional CNN model, a CNN-based transfer learning model, MobileNet-V2, and our novel PDCNN model. CNN, MobileNet, and the newly proposed PDCNN exhibit remarkable efficacy in identifying bone fractures from X-ray images. The succinct description of each model is given below:

#### 2.3.1. Convolutional neural network

Convolutional neural networks [29], or CNNs, are widely utilized in deep learning network models and computer vision algorithms. Because it can identify patterns in images, this kind of artificial neural network is utilized for image recognition and processing. Convolutional, pooling, and fully connected layers are some of the layers that make it up. The convolutional layer, which makes up the majority of CNN, is where characteristics like forms, edges, and patterns are extracted from the input image by applying filters. One or more fully connected layers are then applied to the output of the pooling layers to classify or predict the image.

#### 2.3.2. MobileNet-V2

MobileNet-V2 is a lightweight convolutional neural network designed for mobile and embedded devices. It improves efficiency with depth wise separable convolutions and inverted residuals with linear bottlenecks [30]. It also incorporates expansion and squeeze-excitation modules for better feature learning. With its streamlined architecture, MobileNet-V2 achieves high accuracy while minimizing computational resources, making it ideal for mobile applications requiring fast and efficient image processing.

#### 2.3.3. Parallel deep convolutional neural network (PDCNN)

A parallel architecture with two convolutional neural networks (PDCNNs) is presented to handle the recognition and classification of bone fractures in X-ray pictures. The suggested architecture entails the following sequence of events: X-ray images with bone fractures are fed into the PDCNNs [31] input layer. To reduce the computational complexity, these images are preprocessed. The input images have been normalized to a 277×227-pixel resolution for training, allowing for differences in pixel widths and heights. The subsequent procedure that helps to simplify complexity is to convert the input images to canny edge detection. The architecture of the PDCNN is then used to classify input X-ray pictures by combining, output, local, and global path. The SoftMax function is used in the output pathway to carry out the classification of bone fractures. Figure 5 shows the PDCNN's structure.

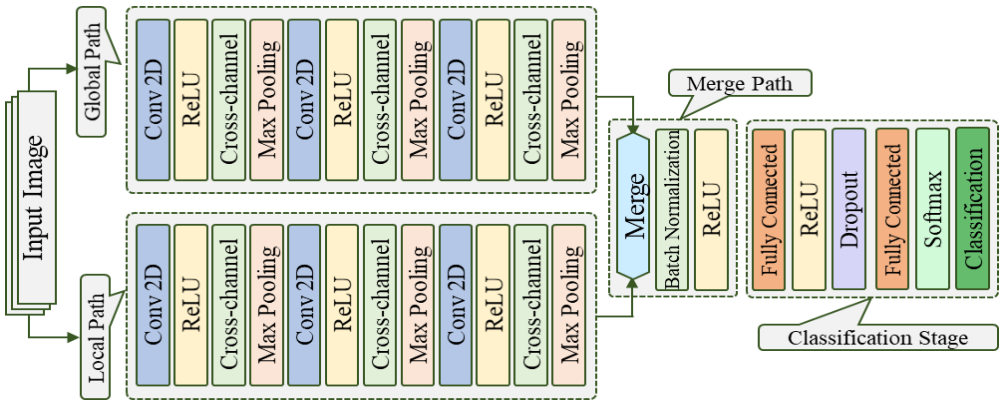


Figure 5. The diagram of proposed PDCNN model that contains four stages which are local path, global path, merging them, and output stages in order to identify the bone fracture from the inputed x-ray image

The proposed PDCNN model for bone fracture identification integrates various layers to facilitate accurate recognition of fractures in X-ray images. Initially, 2D convolutional layers are employed to extract pertinent features from the input images. Subsequently, rectified linear unit (ReLU) layers introduce non-linearity to the network, enhancing its ability to capture complex patterns. A 2D cross-channel normalization layer normalizes activations across channels, contributing to improved model performance. Following this, 2D max pooling layers reduce the dimensionality of feature maps while retaining essential information [32]. Concatenation merges features learned from different pathways within the network, enriching the

representation of fracture-related features. Batch Normalization is applied to accelerate and stabilize the training process, leading to faster convergence and improved generalization. Fully connected layers process high-level features extracted by convolutional layers, enabling the network to generate predictions for fracture identification. Dropout regularization is utilized to mitigate overfitting by randomly dropping units during training. Finally, Softmax activation facilitates robust classification decisions by allowing the network to predict classes based on features extracted through various parallel paths. Table 2 presents the specifications of each layer in the proposed PDCNN model, including the layer type, properties, activation function, learnable property, and number of learnable parameters.

Table 2. The specifications of proposed PDCNN model

| Layer no. | Layer type | Properties | Activation | Learnable property | Number of learnings |
|---|---|---|---|---|---|
| 1 | Image Input | 227×227×3 images with 'zero center' normalization | 227 (S)×227 (S)×227 (S)×3 (C)×1 (B) | - | 0 |
| 2 | 2-D convolution | 32 3×3 convolutions with stride [1×1] and padding 'same' | 227 (S)×227 (S)×32 (C) x×1 (B) | Weight: 3×3×3 Bias: 1×1×32 | 896 |
| 3 | ReLU | ReLU | 227 (S)×227 (S)×32 (C)×1 (B) | - | 0 |
| 4 | Cross-channel normalization | Cross-channel normalization with 5 channels per element | 227 (S)×227 (S)×32 (C)×1 (B) | - | 0 |
| 5 | 2-D Max Pooling | 5×5 max pooling with stride [1×1] and padding 'same' | 227 (S)×227 (S)×32 (C)×1 (B) | - | 0 |
| 6 | 2-D convolution | 32 3×3 convolutions with stride [1×1] and padding 'same' | 227 (S)×227 (S)×32 (C)×1 (B) | Weight: 3×3×32 Bias: 1×1×32 | 9248 |
| 7 | ReLU | ReLU | 227 (S)×227 (S)×32 (C)×1 (B) | - | 0 |
| 8 | Cross-channel Normalization | Cross-channel normalization with 5 channels per element | 227 (S)×227 (S)×32 (C)×1 (B) | - | 0 |
| 9 | 2-D Max Pooling | 5×5 max pooling with stride [1×1] and padding 'same' | 227 (S)×227 (S)×32 (C)×1 (B) | - | 0 |
| 10 | 2-D convolution | 32 3×3 convolutions with stride [1×1] and padding 'same' | 227 (S)×227 (S)×32 (C)×1 (B) | Weight: 3×3×32 Bias: 1×1×32 | 9248 |
| 11 | ReLU | ReLU | 227 (S)×227 (S)×32 (C)×1 (B) | - | 0 |
| 12 | Cross-channel normalization | Cross-channel normalization with 5 channels per element | 227 (S)×227 (S)×32 (C)×1 (B) | - | 0 |
| 13 | 2-D Max Pooling | 5×5 max pooling with stride [1×1] and padding 'same' | 227 (S)×227 (S)×32 (C)×1 (B) | - | 0 |
| 14 | 2-D convolution | 32 3×3 convolutions with stride [1×1] and padding 'same' | 227 (S)×227 (S)×32 (C)×1 (B) | Weight: 3×3×32 Bias: 1×1×32 | 896 |
| 15 | ReLU | ReLU | 227 (S)×227 (S)×32 (C)×1 (B) | - | 0 |
| 16 | Cross-channel normalization | Cross-channel normalization with 5 channels per element | 227 (S)×227 (S)×32 (C)×1 (B) | - | 0 |
| 17 | 2-D Max Pooling | 5×5 max pooling with stride [1×1] and padding 'same' | 227 (S)×227 (S)×32 (C)×1 (B) | - | 0 |
| 18 | 2-D convolution | 32 3×3 convolutions with stride [1×1] and padding 'same' | 227 (S)×227 (S)×32 (C)×1 (B) | Weight: 3×3×32 Bias: 1×1×32 | 9248 |
| 19 | ReLU | ReLU | 227 (S)×227 (S)×32 (C)×1 (B) | - | 0 |
| 20 | Cross-channel normalization | Cross-channel normalization with 5 channels per element | 227 (S)×227 (S)×32 (C)×1 (B) | - | 0 |
| 21 | 2-D Max Pooling | 5×5 max pooling with stride [1×1] and padding 'same' | 227 (S)×22×(S)×32 (C)×1 (B) | - | 0 |
| 22 | 2-D convolution | 32 3×3 convolutions with stride [1×1] and padding 'same' | 227 (S)×227 (S)×32 (C)×1 (B) | Weight: 3×3×32… Bias: 1×1×32 | 9248 |
| 23 | ReLU | ReLU | 227 (S)×227 (S)×32 (C)×1 (B) | - | 0 |
| 24 | Cross-channel normalization | Cross-channel normalization with 5 channels per element | 227 (S)×227 (S)×32 (C)×1 (B) | - | 0 |
| 25 | 2-D Max Pooling | 5×5 max pooling with stride [1×1] and padding 'same' | 227 (S)×227 (S)×32 (C)×1 (B) | - | 0 |
| 26 | Concatenation | Concatenation of 2 inputs along the dimensional value | 227 (S)×454 (S)×32 (C)×1 (B) | - | 0 |
| 27 | Batch Normalization | Batch normalization | 227 (S)×454 (S)×32 (C)×1 (B) | Offset: 1×1×32 Scale: 1×1×32 | 64 |
| 28 | ReLU | ReLU | 227 (S)×454 (S)×32 (C)×1 (B) | - | 0 |
| 29 | Fully connected | 10 fully connected layers | 1 (S)×1 (S)×10 (C)×1 (B) | Weights 10×3297… Bias 10×1 | 32978570 |
| 30 | ReLU | ReLU | 1 (S)×1 (S)×10 (C)×1 (B) | - | 0 |
| 31 | Dropout | 50% dropout | 1 (S)×1 (S)×10 (C)×1 (B) | - | 0 |
| 32 | Fully Connected | 10 fully connected layers | 1 (S)×1 (S)×10 (C)×1 (B) | Weights 10×10 Bias 10×1 | 110 |
| 33 | Softmax | Softmax | 1 (S)×1 (S)×10 (C)×1 (B) | - | 0 |

### 2.4. Performance evaluation

After implementing the model, various performance metrics are calculated to assess its effectiveness in a binary classification task of identifying bone fractures in X-ray images. The first step involves generating a confusion matrix, then key metrics such as true-positive rate, false-negative rate, false-positive rate, and true-negative rate are derived. Following this, accuracy, precision, F1 score, and error are computed to determine the optimal model for bone fracture identification. Their equations "(1)-(8)" are given below:

$$Accuracy = \frac{True\ Positive + True\ Negative}{Total\ no.of\ sample} \times 100\% \quad (1)$$

$$TPR = \frac{True\ Positive}{True\ Positive + False\ Negative} \times 100\% \quad (2)$$

$$FNR = \frac{False\ Negative}{True\ Positive + False\ Negative} \times 100\% \quad (3)$$

$$FPR = \frac{False\ Positive}{False\ Positive + True\ Negative} \times 100\% \quad (4)$$

$$TNR = \frac{True\ Negative}{False\ Positive + True\ Negative} \times 100\% \quad (5)$$

$$Precision = \frac{True\ Positive}{True\ Positive + False\ Positive} \times 100\% \quad (6)$$

$$F_1 Score = \frac{2 \times Precision \times Recall}{Precision + Recall} \times 100\% \quad (7)$$

$$Error\ Rate = \frac{False\ Negative + False\ Positive}{Total\ no.\ of\ samples} \times 100\% \quad (8)$$

## 3. RESULTS AND DISCUSSION

In this study, three deep learning models explore the detection of bone fractures from digital images. Rigorous image preprocessing is applied to train and validate the models using a testing dataset. To measure the performance of the developed models, several performance metrics are computed to find the optimal solution. The three models are trained with 8,884 images and validated with 1,899 images. During the implementation phase, some cases of ablation study are carried out to determine the best-suited parameters for the proposed model. The models are implemented using 100 epochs and a batch size of 64. However, in the case of the traditional CNN and the pretrained MobileNet-V2 model, performance is not satisfactory, and issues arise during the implementation phase. Consequently, a newly developed proposed PDCNN model performs very well. Four ablation case studies are considered to validate the proposed model for bone fracture identification. The performance of these studies is detailed below:

### 3.1. Performance of CNN and MobileNet-V2

In terms of performance, both the traditional CNN and MobileNet-V2 models exhibit fluctuating results, indicating underfitting issues. The confusion matrices of the CNN and MobileNet-V2 models are presented in Table 3 and performance metrices shwon in Table 4. From Table 4, CNN provide 74.51% accuracy while MobileNet-V2 gained 81.20% accuracy. Examination of Figure 6(a) and 6(b) and Figure 7(a) and 7(b) reveals accuracy (Figure 6(a) and Figure 7(a) and loss curves (Figure 6(b) and Figure 7(b) that further emphasize the underfitting problems experienced by both models CNN and MovileNet-V2, respectviely. Underfitting occurs when a model is unable to capture the underlying patterns in the data, resulting in poor performance and low accuracy. In the case of the traditional CNN and MobileNet-V2 models, this underfitting phenomenon is evident in their inability to adequately learn from the training data, leading to inconsistent and suboptimal results.

Table 3. Confusion matrix for applied three models

| Model | TP | FN | FP | TN |
|---|---|---|---|---|
| CNN | 769 | 370 | 114 | 646 |
| MobileNet-V2 | 853 | 266 | 105 | 689 |
| PDCNN | 941 | 84 | 51 | 823 |

Table 4. Performance metrices for CNN and MobileNet-V2 model

| Model | Accuracy | TPR | FNR | FPR | TNR | Precision | F1 Score | Error rate |
|---|---|---|---|---|---|---|---|---|
| CNN | 74.51 | 67.52 | 32.48 | 15.00 | 85.00 | 87.09 | 76.06 | 25.49 |
| MobileNet-V2 | 81.20 | 76.23 | 23.77 | 13.22 | 86.78 | 89.04 | 82.14 | 19.54 |

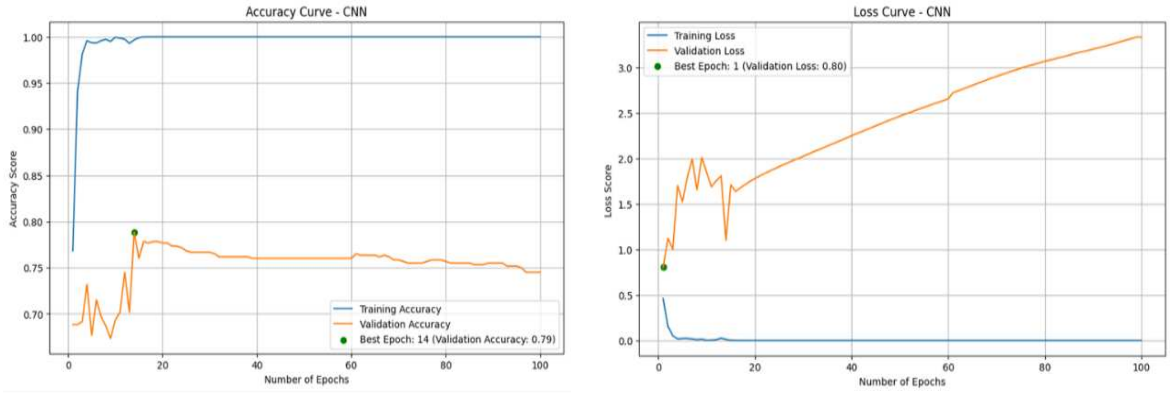


(a) (b)

Figure 6. The (a) accuracy graph and (b) loss graph for traditional CNN model

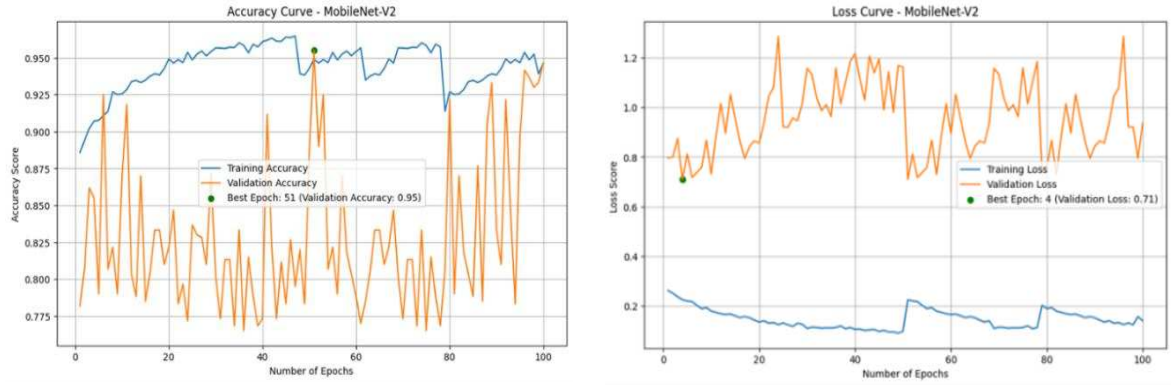


(a) (b)

Figure 7. The (a) accuracy graph and (b) loss graph for MobileNet-V2 model

### 3.2. Performance of proposed PDCCN model with ablation study

In the preceding section, both models failed to deliver satisfactory results. Now, it's imperative to validate the proposed model to demonstrate that the newly developed PDCNN model serves as the optimal solution for bone fracture detection. In the validation process, four detailed case studies are conducted by altering hyperparameters such as kernel size, loss function, pooling layer, and optimizer. The results of the ablation study are presented in Table 5. This comprehensive analysis aims to ascertain the effectiveness of the proposed model in detecting bone fractures and to identify the optimal configuration for achieving the highest performance.

From the ablation studies in Table 5, various convolutional layer kernel sizes have been investigated. Four kernel sizes (2, 3, 4, and 5) are compiled and evaluated. Notably, a kernel size of 3 achieved the maximum accuracy, reaching 88.61%, with a relatively low per-epoch training time of 127 seconds. As a result, a kernel size of 3 is selected for implementation in the PDCNN model. To optimize performance, different loss functions are evaluated, including binary cross-entropy, categorical cross-entropy, and mean squared error. The model attained its highest test accuracy of 89.65% when utilizing the categorical cross-entropy loss function. Consequently, this loss function is chosen for integration into the final model.Further experimentation involved comparing max-pooling and average pooling layers. It is found that the model achieved its peak performance with the max-pooling layer, resulting in an accuracy of 90.47%. Moreover, the optimization process included testing four distinct optimizers—SGD, Adam, RMSprop, and

Adamax—each with a learning rate of 0.001 and a batch size of 64. Remarkably, the highest test accuracy of 92.89% is achieved by adam optimizer, surpassing all previous tuning efforts.

After meticulous parameter tuning and selection, the final model showcased satisfactory performance. Subsequently, fine-tuning parameters are considered to refine the PDCNN model, and the performance metrics are presented in Table 6. Figure 8 illustrates the accuracy and loss curves for the PDCNN model, demonstrating a lack of overfitting or underfitting during training, see Figure 8(a) and Figure 8(b). Both the training and validation curves smoothly converge, with minimal disparity between them. Furthermore, the loss curves steadily decrease from the initial to the final epoch, maintaining a small gap throughout. This stability in the convergence of accuracy and loss curves underscores the robustness and effectiveness of the developed PDCNN model in bone fracture detection.

Table 5. Performance results of four case of abalation studies

| Ablation Study | Configuration | Parameter | Epoch×Time | Test Accuracy | Finding |
|---|---|---|---|---|---|
| Changing kernel size | 1 | 2 | 100×127 s | 87.34% | Improved |
| | 2 | 3 | 100×127 s | 88.61% | Improved |
| | 3 | 4 | 100×152 s | 86.51% | Droped |
| | 4 | 5 | 100×163 s | 82.47% | Droped |
| Changing the loss function | 1 | Binary cross-entropy loss | 100×124 s | 87.19% | Droped |
| | 2 | Categorical cross-entropy | 100×124 s | 89.65% | Improved |
| | 3 | Mean squared error | 100×124 s | 84.27% | Droped |
| Changing pooling layer | 1 | Max | 100×124 s | 90.47% | Improved |
| | 2 | Average | 100×124 s | 88.14% | Droped |
| Changing optimizer | 1 | SGD | 100×124 s | 88.31% | Drop |
| | 2 | Adam | 100×124 s | 92.89% | Highest |
| | 3 | RMSprop | 100×124 s | 91.56% | Droped |
| | 4 | Adamax | 100×124 s | 90.47% | Droped |

Table 6. Performance metrices for proposed PDCNN model

| Model | Accuracy | TPR | FNR | FPR | TNR | Precision | F1 Score | Error rate |
|---|---|---|---|---|---|---|---|---|
| PDCNN | 92.89 | 91.80 | 8.20 | 5.84 | 94.16 | 94.86 | 93.31 | 7.11 |

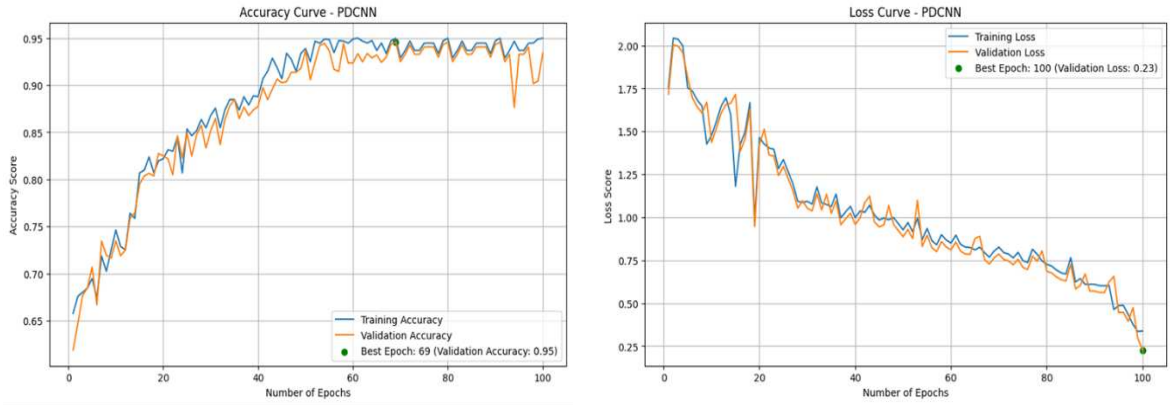


(a) (b)

Figure 8. The (a) accuracy graph and (b) loss graph for proposed PDCNN model

### 3.3. Comperative analysis and discussions

In comparison with previous studies presented in Table 7, our study surpasses the performance achieved by earlier works in bone fracture recognition. Notably, our proposed PDCNN model outperforms all previously reported methods. This remarkable achievement underscores the effectiveness and advancement of our approach in accurately detecting bone fractures.To maintain methodological coherence, we incorporated the canny edge detection image preprocessing technique alongside augmented images. Additionally, we conducted rigorous validation of the proposed model through ablation studies. These efforts collectively contributed to significant improvements in accuracy ranging from 1.89% to 17.89%. Such substantial enhancements highlight the success of our study in pushing the boundaries of bone fracture detection capabilities.

Table 7. Comparision table of earlier work on bone fracture recognition

| Studies | Dataset | Preprocessing Technique | Augmentation | Ablation Study | Model | Accuracy | Performance Gain |
|---|---|---|---|---|---|---|---|
| [9] | 44 | Canny edge detection | × | × | SNAKE | 89% | 3.89% |
| [10] | 40 | Sobel edge detector | × | × | Meta Classifier | 85% | 7.89% |
| [11] | 30 | Sobel edge detector | × | × | SVM | 87.5% | 5.39% |
| [12] | NM | discrete wavelet transforms | × | × | CNN | 79% | 13.89% |
| [13] | 300 | NM | × | × | WFP | 84% | 8.89% |
| [15] | 300 | M3 filter | × | × | SIFT + BPNN | 90% | 2.89% |
| [16] | 900 | Canny edge detection and Conservative Filtering | × | × | BPNN | 91% | 1.89% |
| [17] | 20 | NM | × | × | HTM | 75% | 17.89% |
| [20] | 270 | Canny edge detection | × | × | SVM | NM | N/A |
| This Study | 10,783 | Canny edge detection | ✓ | ✓ | PDCNN | 92.89% | N/A |

a. NM: Not mentioned
b. N/A: Not application

## 4. CONCLUSION

This research marks a significant advancement in the field of medical image analysis by evaluating the effectiveness of various CNN architectures in detecting bone fractures. Our study highlights the crucial role of customized neural network designs specifically tailored to meet the complex requirements of medical imaging tasks. Among the models tested, the PDCNN stood out, demonstrating superior performance compared to MobileNetV2 and traditional CNNs. Through rigorous validation, including four ablation studies, PDCNN consistently achieved higher accuracy, precision, and F1-Score. This model's innovative architectural enhancements were pivotal in addressing the intricate details of bone fracture detection, resulting in its exceptional ability to clearly differentiate between fractured and non-fractured bones. Pre-processing techniques such as segmentation, edge detection, and feature extraction further enhanced the model's diagnostic capabilities. The success of PDCNN suggests that it can significantly improve the accuracy and reliability of bone fracture diagnoses, which is a notable milestone in medical research. This model's simplicity combined with its high accuracy promises substantial advancements in current diagnostic practices, potentially transforming the way bone fractures are identified from X-ray images. The practical implementation of PDCNN could streamline the diagnostic process, reducing reliance on manual identification and thereby saving time and resources in clinical settings. Moreover, the underperformance of traditional CNN and MobileNetV2 models, which exhibited underfitting issues, indicates that further research and refinement are necessary to optimize neural network architectures for medical applications. Our findings underscore the importance of developing and employing customized neural networks to enhance diagnostic accuracy. This research highlights the potential for these advancements to improve healthcare outcomes by enabling more precise and efficient diagnosis of bone fractures. Overall, this study not only contributes to a deeper understanding of CNN applications in medical imaging but also paves the way for future innovations that could revolutionize medical diagnostics.

## REFERENCES

[1] S. Y. Nottestad, J. J. Baumel, D. B. Kimmel, R. R. Recker, and R. P. Heaney, "The proportion of trabecular bone in human vertebrae," *Journal of Bone and Mineral Research*, vol. 2, no. 3, pp. 221–229, Jun. 1987, doi: 10.1002/jbmr.5650020309.
[2] J. Behera, J. Ison, S. C. Tyagi, and N. Tyagi, "The role of gut microbiota in bone homeostasis," *Bone*, vol. 135, p. 115317, Jun. 2020, doi: 10.1016/j.bone.2020.115317.
[3] B. Wildemann *et al.*, "Non-union bone fractures," *Nature Reviews Disease Primers*, vol. 7, p. 57, Aug. 2021, doi: 10.1038/s41572-021-00289-8.
[4] G. L. Koons, M. Diba, and A. G. Mikos, "Materials design for bone-tissue engineering," *Nature Reviews Materials*, vol. 5, no. 8, pp. 584–603, Jun. 2020, doi: 10.1038/s41578-020-0204-2.
[5] S. Zilioli and F. Renolfi, "Micro-compressive testing and synchrotron-based damage analysis of human trabecular bone," M.S. thesis, Dept. Materials Engineering and Nanotechnology, Politecnico Milano, Italy, 2021.
[6] L. Tanzi, E. Vezzetti, R. Moreno, and S. Moos, "X-ray bone fracture classification using deep learning: a baseline for designing a reliable approach," *Applied Sciences*, vol. 10, no. 4, p. 1507, Feb. 2020, doi: 10.3390/app10041507.
[7] T. Meena and S. Roy, "Bone fracture detection using deep supervised learning from radiological images: a paradigm shift," *Diagnostics*, vol. 12, no. 10, p. 2420, Oct. 2022, doi: 10.3390/diagnostics12102420.
[8] T. J. de Villiers and S. R. Goldstein, "Bone health 2022: an update," *Climacteric*, vol. 25, no. 1, pp. 1–3, Jan. 2022, doi: 10.1080/13697137.2021.1965408.
[9] P. H. S. Kalmet *et al.*, "Deep learning in fracture detection: a narrative review," *Acta Orthopaedica*, vol. 91, no. 2, pp. 215–220, Jan. 2020, doi: 10.1080/17453674.2019.1711323.
[10] A. M. Raisuddin *et al.*, "Critical evaluation of deep neural networks for wrist fracture detection," *Scientific Reports*, vol. 11, no. 1, Mar. 2021, doi: 10.1038/s41598-021-85570-2.
[11] L. Nascimento and M. G. Ruano, "Computer-aided bone fracture identification based on ultrasound images," in *2015 IEEE 4th Portuguese Meeting on Bioengineering (ENBENG)*, Feb. 2015, pp. 1–6, doi: 10.1109/enbeng.2015.7088892.
[12] T. Anu, M. Mallikarjunaswamy, and R. Raman, "Detection of bone fracture using image processing methods," *National*

*Conference on Power Systems and Industrial Automation*, vol. 8, no. 3, pp. 6–9, 2015.
[13] A. M. Tripathi, A. Upadhyay, A. S. Rajput, A. P. Singh, and B. Kumar, "Automatic detection of fracture in femur bones using image processing," in *2017 International Conference on Innovations in Information, Embedded and Communication Systems (ICIIECS)*, Mar. 2017, pp. 1–5, doi: 10.1109/iciiecs.2017.8275843.
[14] S. S. Sinthura, Y. Prathyusha, K. Harini, Y. Pranusha, and B. Poojitha, "Bone fracture detection system using CNN algorithm," in *2019 International Conference on Intelligent Computing and Control Systems (ICCS)*, May 2019, pp. 545–549, doi: 10.1109/iccs45141.2019.9065305.
[15] M. Vasilakakis, V. Iosifidou, P. Fragkaki, and D. Iakovidis, "Bone fracture identification in X-ray images using fuzzy wavelet features," in *2019 IEEE 19th International Conference on Bioinformatics and Bioengineering (BIBE)*, Oct. 2019, pp. 726–730, doi: 10.1109/bibe.2019.00136.
[16] D. P. Yadav and S. Rathor, "Bone fracture detection and classification using deep learning approach," in *2020 International Conference on Power Electronics & IoT Applications in Renewable Energy and its Control (PARC)*, Feb. 2020, pp. 282–285, doi: 10.1109/parc49193.2020.236611.
[17] L. J. Rao, P. Neelakanteswar, M. Ramkumar, A. Krishna, and C. Z. Basha, "An effective bone fracture detection using bag-of-visual-words with the features extracted from SIFT," in *2020 International Conference on Electronics and Sustainable Communication Systems (ICESC)*, Jul. 2020, pp. 6–10, doi: 10.1109/icesc48915.2020.9156035.
[18] S. Karimunnisa, P. R. Savarapu, R. K. Madupu, C. Z. Basha, and P. Neelakanteswara, "Detection of bone fractures automatically with enhanced performance with better combination of filtering and neural networks," in *2020 Second International Conference on Inventive Research in Computing Applications (ICIRCA)*, Jul. 2020, pp. 189–193, doi: 10.1109/icirca48905.2020.9183085.
[19] S. J. Pathare, R. P. Solkar, and G. D. Nagare, "Detection of fractures in long bones for trauma centre patients using hough transform," in *2020 International Conference on Communication and Signal Processing (ICCSP)*, Jul. 2020, pp. 88–91, doi: 10.1109/iccsp48568.2020.9182222.
[20] A. Bekkanti, S. Karimunnisa, S. Gogulamudi, K. Kumar, and C. Zeelan Basha, "Enhanced computerized bone fracture detection using harris corner detection," in *2020 International Conference on Smart Electronics and Communication (ICOSEC)*, Sep. 2020, pp. 572–576, doi: 10.1109/icosec49089.2020.9215240.
[21] P. Samothai, P. Sanguansat, A. Kheaksong, K. Srisomboon, and W. Lee, "The evaluation of bone fracture detection of YOLO series," in *2022 37th International Technical Conference on Circuits/Systems, Computers and Communications (ITC-CSCC)*, Jul. 2022, pp. 1054–1057, doi: 10.1109/itc-cscc55581.2022.9895016.
[22] K. Dlshad Ahmed and R. Hawezi, "Detection of bone fracture based on machine learning techniques," *Measurement: Sensors*, vol. 27, p. 100723, Jun. 2023, doi: 10.1016/j.measen.2023.100723.
[23] Y. Rakesh and A. Akilandeswari, "Bone fracture detection using morphological and comparing the accuracy with genetic algorithm," *Journal of Pharmaceutical Negative Results*, vol. 13, pp. 270–276, 2022, doi: 10.47750/pnr.2022.13.S04.030.
[24] H.-Z. Wu *et al.*, "The feature ambiguity mitigate operator model helps improve bone fracture detection on X-ray radiograph," *Scientific Reports*, vol. 11, no. 1, Jan. 2021, doi: 10.1038/s41598-021-81236-1.
[25] A. K. Bitto, M. H. I. Bijoy, S. Yesmin, I. Mahmud, M. J. Mia, and K. B. B. Biplob, "Tumor-Net: convolutional neural network modeling for classifying brain tumors from MRI images," *International Journal of Advances in Intelligent Informatics*, vol. 9, no. 2, p. 148, Apr. 2023, doi: 10.26555/ijain.v9i2.872.
[26] A. Pramanik, F. Chowdhury, S. Sultana, M. M. Rahman, M. H. I. Bijoy, and M. S. Rahman, "Monkeypox detection from various types of poxes: a deep learning approach," in *2023 IEEE 8th International Conference for Convergence in Technology (I2CT)*, Apr. 2023, pp. 1–7, doi: 10.1109/i2ct57861.2023.10126223.
[27] A. A. Q. Amir and I. L. Ahmad, "Computer aided system using canny edge for long bone fracture detection," *Evolution in Electrical and Electronic Engineering*, vol. 3, no. 2, pp. 695–704, 2022.
[28] M. Tennyson, M. Krkovic, M. Fortune, and A. Abdulkarim, "Systematic review on the outcomes of poller screw augmentation in intramedullary nailing of long bone fracture," *EFORT Open Reviews*, vol. 5, no. 3, pp. 189–203, Mar. 2020, doi: 10.1302/2058-5241.5.190040.
[29] A. R. Goyal, A. Mehta, and H. Goel, "Bone fracture detection using convolutional neural networks," *IJNRD - International Journal of Novel Research and Development*, vol. 9, no. 4, pp. h765–h774, 2024.
[30] M. Fradi, M. Afif, and M. Machhout, "Deep learning based approach for bone diagnosis classification in ultrasonic computed tomographic images," *International Journal of Advanced Computer Science and Applications*, vol. 11, no. 12, 2020, doi: 10.14569/ijacsa.2020.0111210.
[31] N. Kheradmandi and V. Mehranfar, "A critical review and comparative study on image segmentation-based techniques for pavement crack detection," *Construction and Building Materials*, vol. 321, p. 126162, Feb. 2022, doi: 10.1016/j.conbuildmat.2021.126162.
[32] T. Rahman and M. S. Islam, "MRI brain tumor detection and classification using parallel deep convolutional neural networks," *Measurement: Sensors*, vol. 26, p. 100694, Apr. 2023, doi: 10.1016/j.measen.2023.100694.

## BIOGRAPHIES OF AUTHORS

**Md. Hasan Imam Bijoy** (member at IEEE, ACM) is a lecturer of Computer Science and Engineering Department at Daffodil International University (DIU), Dhaka, Bangladesh. He has pursued his bachelor's degree in computer science and engineering (CSE) from Daffodil International University. He is a convener of the virtual multidisciplinary research Lab (VMDRL). He is a research zealot, having published over 25 conference papers, 10+ reputed journal publications, and one programming book (A Handbook of C Programming with Example). He has performed the role of reviewer at Telematics and informatics, behavior & information technology, financial innovation, complexity, ICECET2021-22-23, ICECCME2021-22-23 and so many. His area of interest includes health informatics, mHealth, machine learning, deep learning, computer vision, natural language processing, image processing, internet of things, and so many fields. He can be contacted at email: hasan15-11743@diu.edu.bd.

**Nusrat Islam Kohinoor** pursued her bachelor's degree (B.Sc.) in computer science and engineering (CSE) at Leading University, Sylhet. Currently, she is working as an intern software engineer at SJ Innovations, Sylhet. She is also working as an undergraduate research assistant in the InteX Research Lab. Her area of interest in the research field includes machine learning, deep learning, and image processing. She can be reached at: nusrathislamkohinoor@gmail.com.

**Syeda Zarin Tasnim** attended Leading University in Sylhet to complete her bachelor's degree (B.Sc.) in computer science and engineering (CSE). She is employed as a teaching assistant at Anandaniketan School in Sylhet at the moment. She is employed by InteX Research Lab as an undergraduate research assistant as well. Image processing, deep learning, and machine learning are some of the study topics she is interested in. Her email address is: syedazarin00@gmail.com.

**Md. Saidur Rahman Kohinoor** is a senior lecturer in the Department of Computer Science and Engineering at Leading University, Sylhet, Bangladesh, with prior roles as a research associate and lecturer at Daffodil International University, Dhaka, Bangladesh. He is a promising young researcher focused on the application of machine learning, specifically in the areas of healthcare and communications, as well as mobile sensing, context-aware computing, intelligent systems, information and knowledge management, and bioinformatics. As the principal investigator at InteX Research Lab, he leads a team of 34 research enthusiasts, exploring innovative solutions. Driven by a commitment to excellence, he has received several research grants from reputed organizations including the British Council and the Center for Research, Innovative Studies, and Planning (CRISP). In 2018, he was honored as a Richard E. Merwin Scholar of the IEEE Computer Society, recognizing his community-driven contributions. Currently serving as a divisional coordinator at the IEEE CS Bangladesh Chapter to uphold the motto "advancing technology for humanity". He can be contacted at email: kohinoor_cse@lus.ac.bd.